Resonant-cavity-enhanced p-i-n photodiode with a broad quantum-efficiency spectrum by use of an anomalous-dispersion mirror

Chyong-Hua Chen, Kevin Tetz, and Yeshaiahu Fainman

A resonant-cavity-enhanced photodiode with broad filter transmittance and high quantum efficiency was numerically designed and analyzed, fabricated, and validated experimentally. We show theoretically that the quantum-efficiency spectrum broadens because of anomalous dispersion of the reflection phase of a mirror in the device and describe conditions that allow maximal flatness of the transmitted spectrum to be achieved. To demonstrate the concepts we design, fabricate, and characterize a backilluminated $In_{0.47}Ga_{0.53}As$-based p-i-n photodiode upon a InP substrate. Experimental measurements of the fabricated devices demonstrate a peak quantum efficiency of 0.80 at 1550 nm and a FWHM of transmittance of 35.96 nm.

OCIS codes: 040.5160, 230.5160, 230.5170, 230.5750, 310.1620.

1. Introduction

High-speed and high-sensitivity resonant-cavity-enhanced (RCE) photodetectors (PDs) are promising devices for free-space optical communication, optical interconnects, metrology, and optical sensing applications.[1–5] Insertion of a photosensitive active medium within a Fabry–Perot resonant (FPR) cavity enhances the detection quantum efficiency as a result of multiple reflections between the two mirrors of the FPR cavity, effectively increasing the absorption depth of the active medium. Additionally, the FPR cavity can be designed to have a narrowband spectral transmittance to satisfy a specific application. However, for certain applications (e.g., high-speed telecommunications) that require a broader-band flat-topped transmittance for wide angular bandwidth (e.g., free-space communications), a RCE PD built with a simple FPR filter will be limited because of its high wavelength sensitivity as a result of the narrow transmittance function determined by the characteristics of the cavity (length, mirror reflectivity) and its high sensitivity to angular bandwidth because of the strong angular dependence of the FPR resonance at a given wavelength. Moreover, fabrication of such a RCE detector will be challenging because it will be difficult to meet the tolerance requirements for aligning the resonance frequency. Therefore the first design rule of a RCE detector is to widen the wavelength sensitivity band of the FPR filter to create ideal flattopped quantum efficiency while maintaining the resonance enhancement of the photodetection by the cavity.

Several approaches to achieving broad spectral quantum efficiency by introducing a cavity into the incident distributed Bragg mirror (DBM) have been investigated. Design examples include depositing a half-wave thickness layer onto the DBM[6] and introducing an additional coupling mirror between the DBM and the active layer.[7,8] However, these approaches were based on numerical simulation. In Ref. 6 a device operating at a wavelength of 850 nm is described, but a detailed design and the trade-offs among the various parameters are not given. The results of Refs. 7 and 8 are based on computer simulations, and the proposed devices have not yet been fabricated and experimentally demonstrated. In this paper we analytically derive the design rules for achieving a RCE PD with flattopped spectral response and provide an experimental demonstration of such a device working in the telecommunication spectral band. We show that the shape of the quantum-efficiency spectrum (or response) can be controlled by engineering the reflection phase prop-

The authors are with the Department of Electrical and Computer Engineering, University of California, San Diego, 9500 Gilman Drive, La Jolla, California 92093-0407. C.-H. Chen's e-mail address is chyong@ece.ucsd.edu.

Received 7 March 2005; revised manuscript received 12 May 2005; accepted 24 May 2005.

0003-6935/05/296131-10$15.00/0

erties of the spacer and the incident mirror, called the entrance mirror. The flattopped passband is obtained when the entrance mirror has an anomalous-dispersion (AD) region in the reflection phase of the mirror. When the design of the mirror satisfies the optimum conditions, flattopped quantum efficiency is obtained and the flatness of the spectral bandwidth is determined by the width of the AD region. We also perform a tolerance analysis to estimate the effect of fabrication inaccuracies on the expected performance of the device.

In Section 2 we present a semianalytical formulation to describe accurately the quantum efficiency of a RCE PD. In addition, we systematically develop an analytic approach to achieving flattopped quantum efficiency of a RCE PD by examining the properties of both mirrors, including spacers and their relation to the thickness of the active layer. In Section 3 we present numerical results of the implementation of a RCE PD with flattopped quantum efficiency and discuss engineering the spectral bandwidth response of the device. In Section 4 we show the effects of variations of design parameters, e.g., variation of the absorption coefficient and properties of materials, on the performance of this RCE PD. In Section 5 we validate our design concepts by describing the fabrication and characterization of a backilluminated RCE p-i-n photodiode. A summary and suggestions for further improvements of the device are given in Section 6.

2. Methods

There exist two methods with which to calculate the quantum efficiency of RCE PDs: One is an analytical formulation presented by Kishino *et al.* in 1991,[1] and the other is a numerical method, called the transfer matrix method (TMM).[2,3] Because they include the standing-wave effect and neglect the reflection at the interfaces between the active layer and surrounding spacers in their model, we need to modify the results obtained with the model of Kishino *et al.*[9–13] The numerical method does not account for losses of the materials except in the active layer and hence is inaccurate when it is applied to a structure with lossy materials for the mirrors. This occurs, for example, when one of the mirrors is metallic, as it is in the case addressed here. Therefore we develop here another semianalytical method with which to describe accurately the quantum efficiency of a conventional p-i-n RCE PD. Instead of calculating the performance of spacers and mirrors separately, we group a spacer and a mirror and then calculate the reflection and transmission properties by using the TMM. By calculating the power absorbed in the active layer, we obtain the quantum efficiency by the ratio of absorbed power P_{absorb} to the input power P_{in}. A detailed analysis is now developed.

A. Analysis

The conventional structure of a RCE device is shown schematically in Fig. 1. The photoabsorptive active layer (i.e., the detector layer), of thickness d, refractive index n_a, and absorption coefficient α, is inserted into a FPR cavity. Active layer C and two spacers, S_1 and S_2, are integrated into a cavity made from two mirrors, M_1 and M_2. Optical fields $\{E_{iR}, E_{iL}\}$ and $\{E_{oR}, E_{oL}\}$ denote waves propagating in the positive and negative z-axis directions from the input and the output regions, respectively. $\{E_{aR}, E_{aL}\}$ describe the traveling waves at the interface between the active layer and left-hand spacer S_2, whereas $\{E_{aR'}, E_{aL'}\}$ represent the traveling waves at the interface between the active layer and right-hand spacer S_1. The relationships between $\{E_{iR}, E_{iL}\}$, $\{E_{aR}, E_{aL}\}$, and $\{E_{aR'}, E_{aL'}\}$, $\{E_{oR}, E_{oL}\}$ can be obtained by the TMM[14] and expressed as

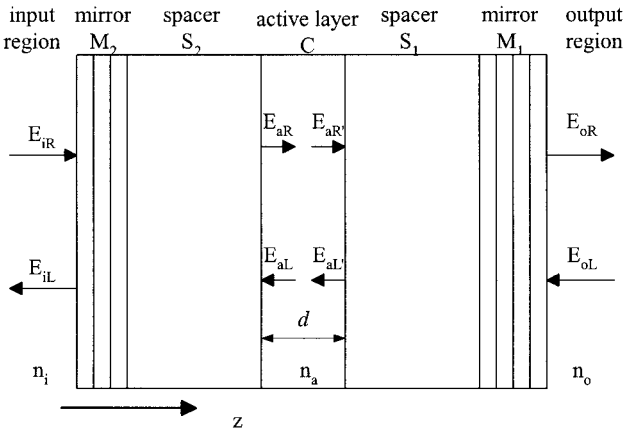

Fig. 1. Schematic of the structure of a generalized RCE photoreceiver.

$$\begin{bmatrix} E_{iR} \\ E_{iL} \end{bmatrix} = \begin{bmatrix} 1/t_{11} & -r_{12}/t_{12} \\ r_{11}/t_{11} & 1/t_{12} \end{bmatrix} \begin{bmatrix} E_{aR} \\ E_{aL} \end{bmatrix},$$

$$\begin{bmatrix} E_{aR'} \\ E_{aL'} \end{bmatrix} = \begin{bmatrix} 1/t_{21} & -r_{22}/t_{22} \\ r_{21}/t_{21} & 1/t_{22} \end{bmatrix} \begin{bmatrix} E_{oR} \\ E_{oL} \end{bmatrix},$$

$$\begin{bmatrix} E_{aR} \\ E_{aL} \end{bmatrix} = \begin{bmatrix} \exp[(\alpha/2 + j\beta)d] & 0 \\ 0 & \exp[-(\alpha/2 + j\beta)d] \end{bmatrix} \times \begin{bmatrix} E_{aR'} \\ E_{aL'} \end{bmatrix}, \quad (1)$$

where $\{t_{11}, r_{11}\}$ and $\{t_{12}, r_{12}\}$ are transmission and reflection coefficients of the multilayer structure of the entrance mirror (i.e., mirror M_2 and spacer S_2), as seen from the input medium and from the active layer medium, respectively. Similarly, $\{t_{21}, r_{21}\}$ and $\{t_{22}, r_{22}\}$ are transmission and reflection coefficients of the structure constructed by the bottom mirror (i.e., spacer S_1 and mirror M_1), as seen from the active layer medium and from the output medium, respectively. Here β is the propagation constant, $\beta = k_o n_a$, where k_o is the wavenumber, $2\pi\lambda^{-1}$, and λ is the wavelength of the optical field.

The total power absorbed in the active layer is[1,2]

$$P_{\text{absorb}} = \frac{n_a}{2\eta_o}\left(|E_{bR}|^2 + |E_{bL'}|^2\right)[1-\exp(-\alpha d)], \quad (2)$$

where η_o is the characteristic impedance of electromagnetic waves in vacuum.

Finally, quantum efficiency η of the RCE PD device can be described by

$$\eta = \frac{P_{\text{absorb}}}{P_{\text{in}}} = \frac{n_a}{n_i}\frac{|t_{11}|^2\left[1+r_{21}{}^2\exp(-\alpha d)\right][1-\exp(-\alpha d)]}{|1-r_{12}r_{21}(t_{11}/t_{12})\exp(-\alpha d-2j\beta d)|^2}. \quad (3)$$

If there is no absorption for materials that form the entrance mirror in the operational spectral bandwidth of the device, then Eq. (3) can be rewritten as

$$\eta(\lambda) = \frac{[1-r_1(\lambda)^2][1+r_2(\lambda)^2\exp(-\alpha d)][1-\exp(-\alpha d)]}{\left\{1+r_1(\lambda)^2r_2(\lambda)^2\exp(-2\alpha d)-2r_1(\lambda)r_2(\lambda)\exp(-\alpha d)\cos[2\beta d-\phi_1(\lambda)-\phi_2(\lambda)]\right\}}, \quad (4)$$

where we use the relations $r_{12} = r_1\exp(j\phi_1)$ and $r_{21} = r_2\exp(j\phi_2)$, r_1 and r_2 are amplitudes of r_{12} and r_{21}, and ϕ_1 and ϕ_2 are their phases.

Compared to the analytical formulation,[1] Eq. (4) is similar, except that the calculation of r_1, r_2, ϕ_1, and ϕ_2 includes the properties of the spacers and mirrors; hence the standing-wave effect is excluded from this model. In addition, as all layers of the structure except the active layer are lossless, Eq. (4) is equivalent to $1 - R - T$, where R and T correspond to the reflectance and transmittance of the whole RCE PD structure; the same formulation is used to calculate the quantum efficiency by TMM.[2]

B. Conditions for Obtaining High Quantum Efficiency with a Flattopped Spectrum

To design a RCE PD that will possess a flattop and high quantum efficiency about center wavelength λ_o we need to control the design parameters to optimize the value of the quantum efficiency. Suppose that the absorption coefficient of the active layer is nondispersive, i.e., that α is independent of wavelength. As Eq. (4) has the same form as the analytical formulation,[1] the maximum quantum efficiency can be obtained if $\Phi(\lambda_o) = 2\beta d - \phi_1(\lambda_o) - \phi_2(\lambda_o) = 2m\pi$ ($m = \ldots -2, -1, 0, 1, 2 \ldots$) and $r_1(\lambda_o) = r_2(\lambda_o) \times \exp(-\alpha d)$.[1] Next, to decrease the wavelength dependence of the quantum efficiency (i.e., flattopped condition), we need to ensure that the second derivative of η be as close to zero as possible near λ_o. We can achieve the latter condition by setting the first derivatives of r_1, r_2, and Φ at λ_o to zero.

Because η increases monotonically with r_2, we require that r_2 have a local maximum with zero first derivative at λ_o to achieve high quantum efficiency. When we closely examine Φ we find that the term $2\beta d$ decreases as the wavelength increases. Because r_2 has a local maximum at λ_o, phase ϕ_2 increases near λ_o as the wavelength increases. Therefore ϕ_1 has to decrease with increasing wavelength to compensate for the phase variation of Φ caused by $2\beta d$ and ϕ_2. A mirror with such a property is an AD mirror[15] and can be part of a nonperiodic multilayered structure. Additionally, to achieve a flattopped passband (i.e., quantum efficiency), we must design r_1 to have a local minimum at center wavelength λ_o to achieve zero value of its first derivative.

We conclude that, to achieve the highest value and a flat passband of quantum efficiency, the conditions (i) $\Phi(\lambda_o) = 2m\pi$, (ii) $r_1(\lambda_o) = r_2(\lambda_o)\exp(-\alpha d)$, and (iii) $d\Phi(\lambda_o)/d\lambda = 0$ have to be simultaneously satisfied. In Section 3 we present several results of simulations, discuss the effects of the entrance mirror designs on the performance of the RCE PDs, and discuss the design for optimal engineering of the bandwidth of such a RCE PD with an AD mirror as the entrance mirror.

3. Numerical Results

A. Materials

To simplify the fabrication and the discussion, we use a metallic mirror as mirror M_1. For compatibility with the fabrication process, gold (Au; $n_{\text{Au}} = 0.559–9.81i$) and titanium (Ti; $n_{\text{Ti}} = 4.04–3.82i$) are chosen.[16] Here, we choose n^+-doped InP ($n_{\text{InP}} = 3.176$), i-$In_{0.53}Ga_{0.47}As$ ($n_{\text{InGaAs}} = 3.6$), and p^+-doped InP for our heterojunction p-i-n PD. The absorption coefficient of $In_{0.53}Ga_{0.47}As$ is $10^4\ \text{cm}^{-1}$. All values are given for a wavelength of 1500 nm. For DBMs of mirror M_2 we choose $In_{0.523}Al_{0.477}As$ ($n_{\text{InAlAs}} = 3.2$) and $In_{0.531}Ga_{0.417}Al_{0.052}As$ ($n_{\text{InGaAlAs}} = 3.5$), with bandgaps at 924 and 1450 nm,[17] respectively. In the following simulation, we set the center wavelength of the design to $\lambda_o = 1560$ nm and the bottom mirror to consist of 294.4 nm thick p^+ InP (S_1), 5 nm thick titanium (M_{1a}), and 500 nm thick gold (M_{1b}) to simplify the discussion. The thicknesses for InAlAs/InGaAlAs (L/H) for the DBMs are 91.3 and 139.4 nm. In addition, S_2 and C represent the thicknesses of the spacer n + InP layer and that of the InGaAs active layer, respectively.

B. Quantum Efficiency with Varying Entrance Mirror Reflection Phase

As discussed above, a flattopped passband is obtained when the entrance mirror has an AD reflection phase. Such a property can be achieved (see Ref. 15) by use of a mirror whose structure is $S_2L(HL)^pH_1H(LH)^qLH_2$, with the condition that $p > q$, where H_1 and H_2 are thicknesses of the InGaAlAs layer and p and q are the numbers of InAlAs/InGaAlAs pairs. In the research reported in Ref. 15, each layer in the structure was either a quarter- or a multiple half-wave thick. Here we generalize the structure to the nonquarter- and nonhalf-waves as follows: The reflection coefficient of the multilayer structure $S_2L(HL)^pH_1(LH)^qLH_2$ can be expressed as[18]

$$\frac{rr_1(\lambda) - rr_2(\lambda)\exp[-j\phi_{11}(\lambda)]}{1 - rr_1(\lambda)rr_2(\lambda)\exp[-j\phi_{11}(\lambda)]}, \tag{5}$$

where rr_1 and rr_2 are the reflection coefficients of DBMs M_{2a}, $(HL)^pLS_2$, and M_{2b}, $(LH)^qLH_2$, respectively. ϕ_{11} is the round-trip phase shift in layer H_1, i.e., $2k_on_1d_1$, where n_1 and d_1 are the refractive index and the thickness of cavity H_1, respectively.

At resonance wavelength λ_o the amplitude of reflection coefficient r_1 is

$$r_1(\lambda_o) = \left| \frac{|rr_1(\lambda_o)| - |rr_2(\lambda_o)|}{1 - |rr_1(\lambda_o)rr_2(\lambda_o)|} \right|. \tag{6}$$

The reflection phase slope of entrance mirror ϕ_1 at λ_o is

$$\frac{d\phi_1}{d\lambda} = \left(\frac{d\phi_A(\lambda_o)}{dk_o} + \frac{|rr_2(\lambda_o)|\left[1 - |rr_1(\lambda_o)|^2\right]}{\left[|rr_1(\lambda_o)| - |rr_2(\lambda_o)|\right]\left[1 - |rr_1(\lambda_o)|\,|rr_2(\lambda_o)|\right]} \times \frac{d\Phi_A}{dk_o} \right) \frac{dk_o}{d\lambda}, \tag{7}$$

where $\Phi_A = \phi_{11} - \phi_A - \phi_B$ and ϕ_A and ϕ_B are phase changes on reflection associated with rr_1 and rr_2. Here we can see that a negative slope is obtained when $|rr_1(\lambda_o)| > |rr_2(\lambda_o)|$, which corresponds to the condition $p > q$.

To achieve the third optimized condition, $d\Phi(\lambda_o)/d\lambda = 0$, we need a derivative of ϕ_1 at λ_o:

$$\frac{d\phi_1}{d\lambda} = \left(2n_ad - \frac{d\phi_2}{dk_o}\right) \frac{dk_o}{d\lambda}. \tag{8}$$

With this mirror as the entrance mirror of the RCE PD, the structure of our design is $H_2L(HL)^qH_1(LH)^pLS_2CS_1M_1$. For example, with an active layer 467.6 nm thick, we analytically obtain a maximum quantum efficiency of 0.84 when the amplitude of the reflection coefficient r_1 of the entrance mirror is 0.538 at λ_o and $\Phi(\lambda_o) = 2m\pi$. There are many combinations of H_2, H_1, S_2, p, and q that satisfy the above specifications, and Fig. 2 shows the simulation results for three examples of entrance mirror designs with conditions $p > q$ ($p = 13$, $q = 7$), $p < q$ ($p = 7$, $q = 14$), and $H_1 = H$ ($p + q = 6$). Figure 2(a) illustrates the relation between r_1 and the values of $r_2\exp(-\alpha d)$. The three mirror designs satisfy the second condition, $r_1(\lambda_o) = r_2(\lambda_o)\exp(-\alpha d)$, and the design for $p > q$ has a spectrum similar to that for $p < q$, whereas the design for $H_1 = H$ corresponds to conventional DBM performance. Figure 2(b) shows that reflection phase ϕ_1 has the desired AD region about λ_o only when $p > q$. Figure 2(c) displays the corresponding total phase [$\Phi(\lambda_o) = 2m\pi$ in all cases]. In addition, for $p < q$, Φ has the steepest variation at λ_o, and, for $p > q$, Φ has approximately zero variation at λ_o; hence we expect that the quantum efficiency for $p > q$ will have a flattopped response because it also satisfies our third condition, that $d\Phi(\lambda_o)/d\lambda = 0$. Figure 2(d) displays the corresponding quantum efficiencies, demonstrating that three designs have the same maximum quantum efficiency of 0.84. Additionally, for $p > q$ a flattopped passband is achieved near λ_o with a steeper edge response than that for $H_1 = H$. The bandwidth at 0.02 dB (99.5%) below the peak is 13.27 nm. On examining reflection phase ϕ_1 [Fig. 2(b)], we found that this value is approximately the same as the width of the AD regions of ϕ_1, 13.62 nm. The quantum efficiency for $p < q$ has the steepest edge response with the narrowest bandwidth. Even though only the entrance mirror has an AD property, a RCE PD possesses a flattopped quantum-efficiency spectrum for which the width of the flatness is close to that of the AD region in the reflection phase.

C. Spectral Bandwidth Engineering

In this subsection we discuss the effect of the design parameters of the $H_2L(HL)^qH_1(LH)^pLS_2CS_1M_1$ structure on the spectral bandwidth of a RCE PD. The flattopped bandwidth of quantum efficiency is nearly the same as the width of the AD region of the entrance mirror's reflection phase. In addition, Ref. 18 shows that the AD region's width can be controlled by the reflectance of DBMs M_{2a} and M_{2b} and by the thicknesses of the spacers that correspond to p, q, and H_1. As a result, different values of p, q, and H_1 of the AD mirrors are chosen to satisfy the optimized conditions, and their properties and performance are shown in Fig. 3. From Fig. 3(a) we can see that all three designs have similar amplitudes of reflection coefficient spectra, except off resonance. In addition, as shown in Fig. 3(b), the total phases Φ in these examples are approximately the same. Hence, as expected, these designs have approximately the same quantum efficiency—except off resonance—as shown in Fig. 3(c). As the reflectance of the AD mirror in the off-resonance state is smaller, a slightly higher quantum efficiency is obtained. These results indicate that the bandwidth of the quantum efficiency is independent of the choices of p, q, and H_1 for a structure of

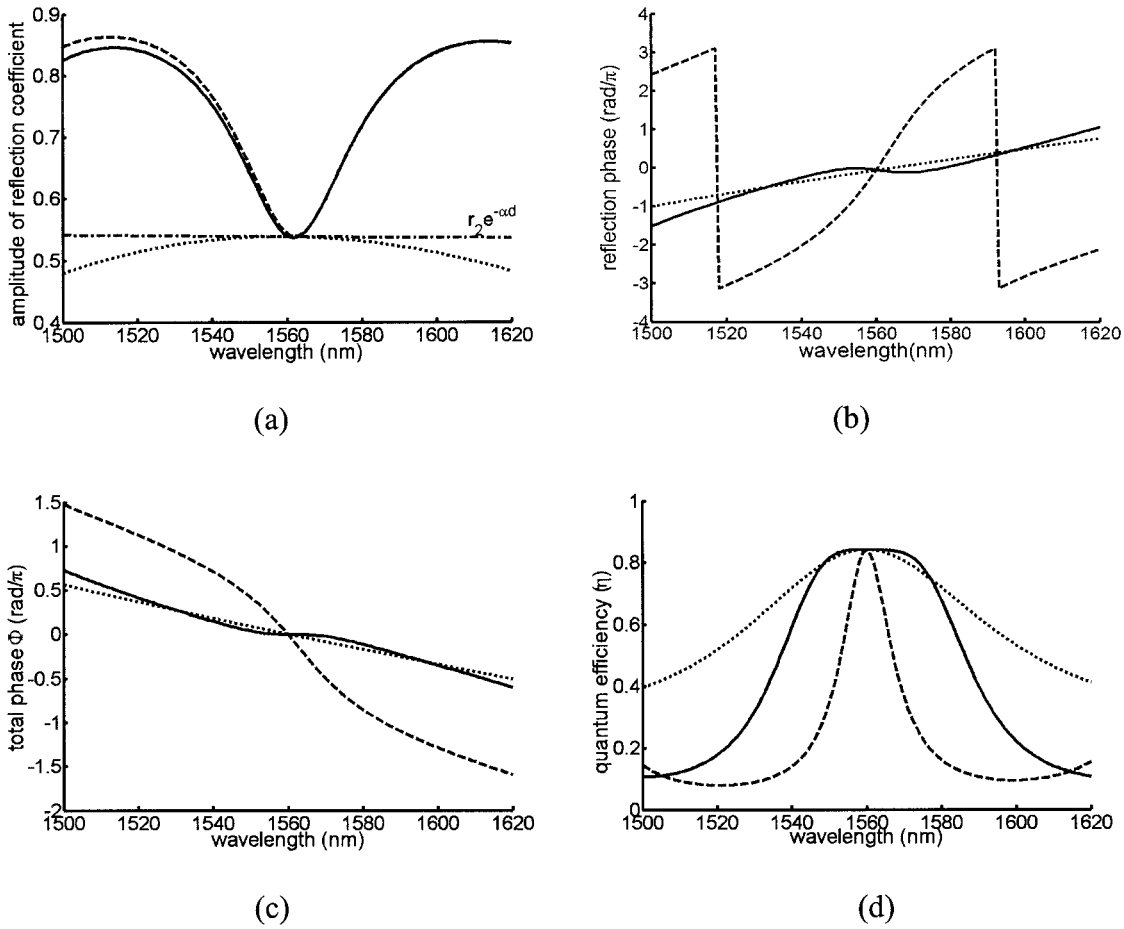

Fig. 2. Results of simulation with three designs of RCE PDs with structure $H_2L(HL)^qH_1(LH)^pLS_2CS_1M_1$, where $p = 13$, $q = 7$, $H_1 = 249$ nm, $H_2 = 69.7$ nm, and $S_2 = 355.8$ nm (solid curves); $p = 7$, $q = 14$, $H_1 = 468.64$ nm, $H_2 = 69$ nm, and $S_2 = 220$ nm (dashed curves); and $p + q = 6$, $H_1 = 139.4$ nm, $H_2 = 61.5$ nm, and $S_2 = 358.3$ nm (dotted curves). Here L and H are 91.3 and 139.4 nm, respectively. (a) Amplitude of the reflection coefficients of the entrance mirror with structure $S_2L(HL)^pH_1(LH)^qLH_2$; the dashed–dotted curve is the curve of $r_2 \exp(-\alpha d)$. (b) Reflection phase of entrance mirror ϕ_1. (c) Total phase shift Φ of RCE PDs. (d) Quantum efficiency of RCE PDs.

$H_2L(HL)^qH_1(LH)^pLS_2CS_1M_1$ with fixed thicknesses of the active layer and the bottom mirror. Subsequently, we investigate the dependence of the maximum quantum efficiency and bandwidth on the thickness of the active layer (see Fig. 4). Here the bandwidth is defined as the FWHM of the quantum efficiency. We observe that both the maximum and the bandwidth of the quantum efficiency increase as thickness d of the active layer increases, showing that the bandwidth is approximately a linearly increasing function.

It is well known that the passband becomes narrower when high-order spacers in thin-film design[19] are used. We investigate these effects first by increasing the length of layer H_1 to operate at a higher-order wavelength. Based on Eq. (7), the consequences of increasing the thickness of H_1 are a decrease of reflection phase ϕ_1 at λ_o and an increase of Φ at λ_o.

Figure 5(a) shows the quantum efficiency with $H_1 = 249$, 1137.9, and 2026.8 nm for RCE PDs with the structure $H_2L(HL)^qH_1(LH)^pLS_2CS_1M_1$, where $p = 13$, $q = 7$, $H_2 = 69.7$ nm, and $S_2 = 355.8$ nm. We see that as H_1 increases, the maximum quantum efficiency is unchanged. However, the FWHM of the transmission bandwidth is reduced, and the curve's edge is rounded. The corresponding widths at 0.02 dB below peak value are 13.27, 9.50, and 5.83 nm. Increasing the thickness of spacer S_2 to a higher-order wavelength results in reducing the phase slope of ϕ_A at λ_o and consequently decreases Φ at λ_o. Figure 5(b) shows the quantum efficiency with $S_2 = 355.8$, 1340.0, 2324.3 nm as $H_1 = 249.0$ nm, showing results similar to those for higher-order H_1. The corresponding widths at 0.02 dB below peak value are 13.27, 8.73, and 5.66 nm. We find that the quantum efficiency does not have a maximally flat passband because the third optimization condition is not satisfied. The discussion above demonstrates that the increase of H_1 and S_2 affects the slope of Φ at the resonant wavelength differently, and for completeness we show in Fig. 5(c) plots of quantum efficiency with different values of H_1 and S_2 that satisfy our third optimization condition. The corresponding widths at 0.02 dB below peak value are 13.27, 9.53, and 7.26 nm. We see that these designs possess not only wider flattopped widths than those with either higher-order H_1 or S_2

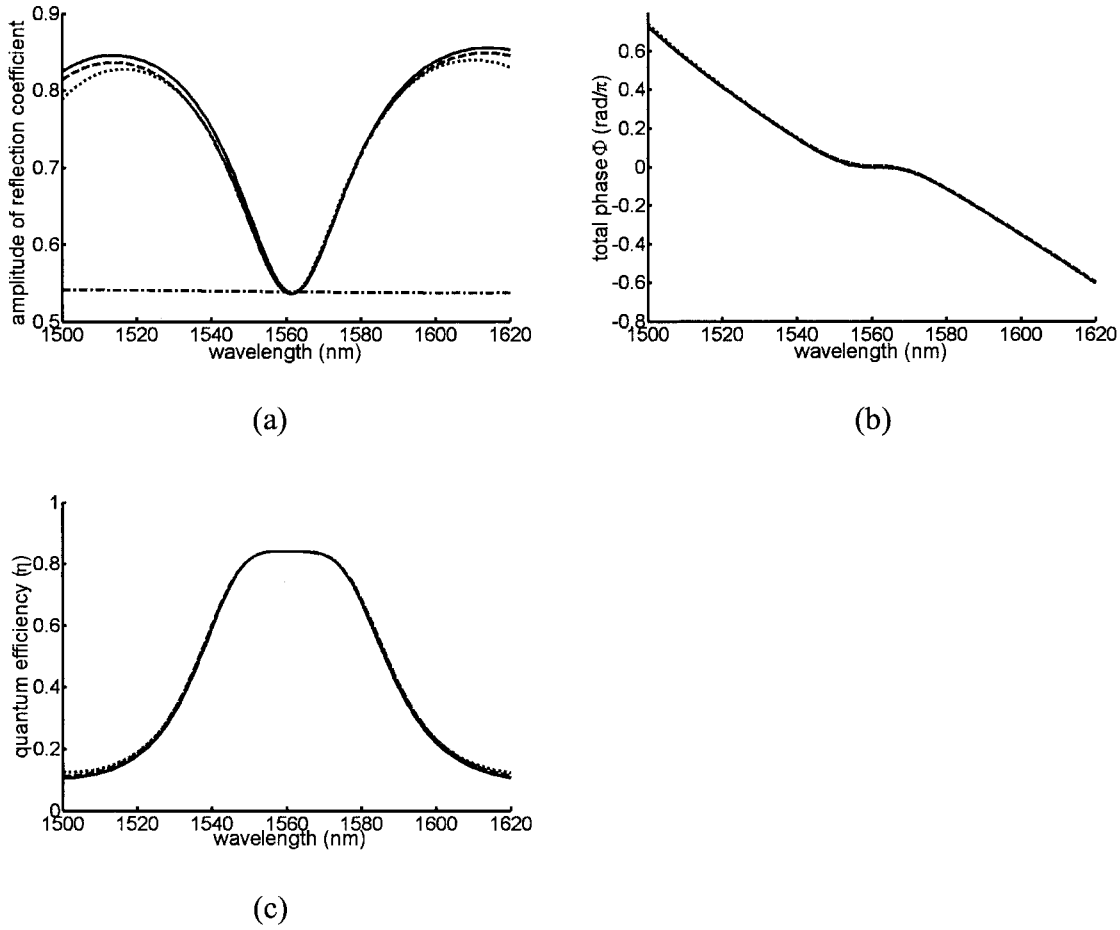

Fig. 3. Performance and the properties of the RCE PDs with structure $H_2L(HL)^qH_1(LH)^pLS_2CS_1M_1$, where $p = 13$, $q = 7$, $H_1 = 249.0$ nm, and $H_2 = 69.7$ nm (solid curves); $p = 12$, $q = 6$, $H_1 = 694.2$ nm, and $H_2 = 69.5$ nm (dashed curve); and $p = 11$, $q = 5$, $H_1 = 1362.3$ nm, and $H_2 = 69.5$ nm (dotted curves). The thickness of active layer C is 467.6 nm, and $S_2 = 355.8$ nm. (a) Corresponding amplitudes of the reflection coefficients of entrance mirrors $S_2L(HL)^pH_1(LH)^qLH_2$. The dashed–dotted curve is the curve of $r_2 \exp(-\alpha d)$. (b) Total phase shift Φ of these three designs. (c) Corresponding quantum efficiency.

but also a steeper edge response. Summarizing, we can adjust the bandwidth of a RCE PD with the structure $H_2L(HL)^qH_1(LH)^p$-$LS_2CS_1M_1$ by varying the thickness of the active layer, cavity H_1, and spacer S_2.

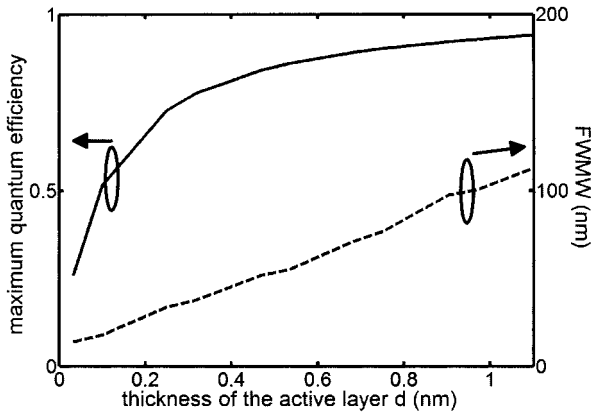

Fig. 4. Maximum quantum efficiency and bandwidth of the RCE PD with structure $H_2L(HL)^qH_1(LH)^pLS_2CS_1M_1$ with variations of the active layer's thickness.

4. Sensitivity of the Design

Under practical conditions the discrepancy between the ideal design and the fabricated device results chiefly from such factors as imperfect materials and inaccurate thickness growth. In what follows, we discuss the sensitivity of our design to these factors for a RCE PD with the structure $H_2L(HL)^qH_1(LH)^pLS_2AS_1M_1$ with $p = 13$, $q = 7$, $H_1 = 249.0$ nm, $H_2 = 69.7$ nm, and $S_2 = 355.8$ nm.

A. Absorption Coefficient of the Active Layer

The variation of α affects primarily the value of $r_2 \exp(-\alpha d)$ and results in mismatching of our second optimization condition, $r_1 = r_2 \exp(-\alpha d)$, at λ_o. Figure 6 shows that the maximum quantum efficiency increases as α increases. However, by calculating the optimized maximal quantum efficiencies with $\alpha = 0.8 \times 10^4$, 1.0×10^4, 1.2×10^4 cm^{-1}, we find that the values obtained at λ_o when $\alpha = 0.8 \times 10^4$, 1.2×10^4 cm^{-1} are slightly smaller than those calculated under the optimized conditions. In addition, the bandwidth of the quantum efficiency is reduced as α increases. When $\alpha = 0.8 \times 10^4$ cm^{-1}, a broader pass-

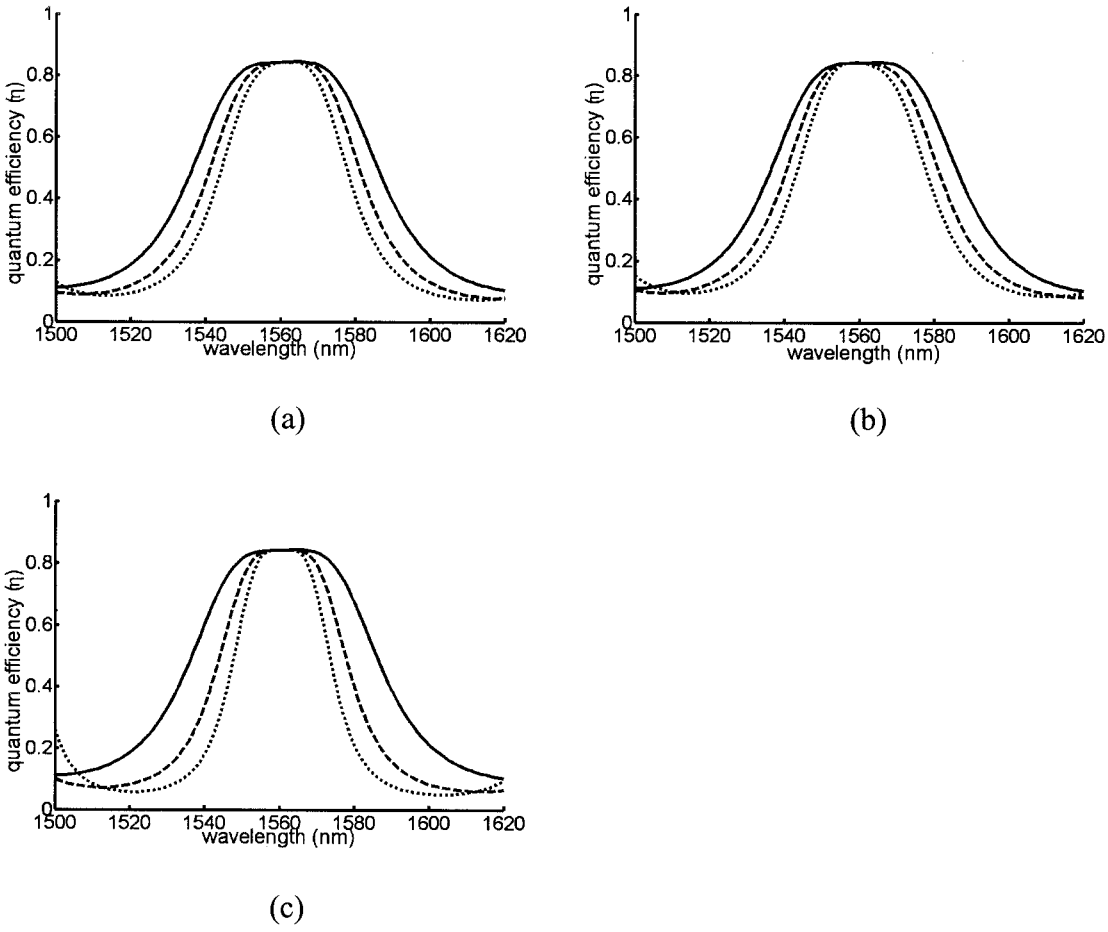

Fig. 5. Quantum efficiency with three orders of cavity thickness H_1 and the spacer S_2. (a) Quantum efficiency of PDs with H_1 = 249.0 nm (solid curve), H_1 = 1137.9 nm (dashed curve), and H_1 = 2026.8 nm (dotted curve). S_2 = 355.8 nm. (b) Quantum efficiency with S_2 = 355.8 nm (solid curve), S_2 = 1340.0 nm (dashed curve), and S_2 = 2324.2 nm (dotted curve). H_1 = 249 nm. (c) Quantum efficiency with H_1 = 249.0 nm and S_2 = 355.8 nm (solid curve), H_1 = 1137.9 nm and S_2 = 1340.0 nm (dashed curve), and H_1 = 2026.8 nm and S_2 = 2324.2 nm (dotted curve).

band with ripples inside is obtained. The ripples occur at the wavelength where $r_1 = r_2 \exp(-\alpha d)$. In contrast, for $\alpha = 1.2 \times 10^4$ cm^{-1} we observe a rounded passband because there is no intersection between r_1 and $r_2 \exp(-\alpha d)$.

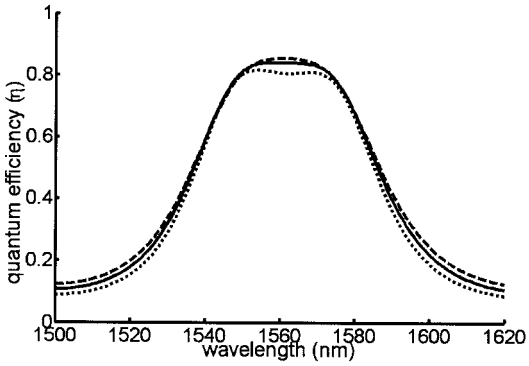

Fig. 6. Quantum efficiency versus absorption coefficient: $\alpha = 1.2 \times 10^4$ cm^{-1} (dashed curve), 1×10^4 cm^{-1} (solid curve), and 0.8×10^4 cm^{-1} (dotted curve).

B. Refractive Indices and Thickness of Dielectric Layers

Next we discuss the sensitivity of our design to variations in refractive index and thickness of DBM M_2. The refractive indices of the materials with alloy compositions vary based on the concentration of the content.[20] Figure 7 shows the spectra of r_1 for various values of InGaAlAs (n_{InGaAlAs}) and InAlAs (n_{InAlAs}) and the corresponding quantum-efficiency spectra. We can see that quantum-efficiency spectra shift to shorter wavelength as the refractive index of InGaAlAs (n_{InGaAlAs}) or InAlAs (n_{InAlAs}) decreases, because decreasing n_{InAlAs} or n_{InGaAlAs} causes the reflectance spectra of M_2 to shift to shorter wavelengths. In addition, decreasing n_{InAlAs} results in an increase of the reflectance of M_2, and thus the spectrum of the quantum efficiency has a narrower and rounder shape because of the absence of an intersection between r_1 and $r_2 \exp(-\alpha d)$. In contrast, the reflectance of M_2 decreases as a result of the decrease of n_{InGaAlAs}; hence the broad quantum efficiency spectrum with ripples is obtained from two intersecting points between r_1 and $r_2 \exp(-\alpha d)$.

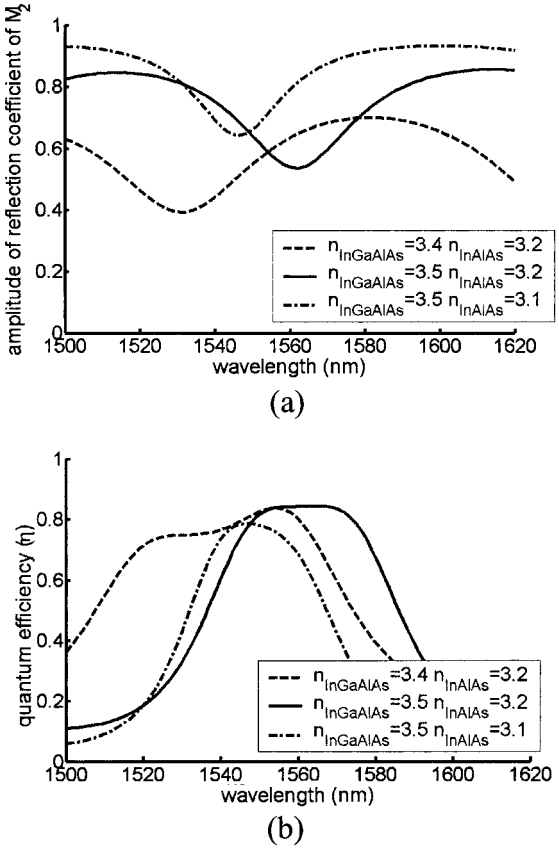

Fig. 7. Effect of variations in the refractive indices of InGaAlAs and InAlAs materials. (a) Amplitude of reflection coefficients r_1 with variations of n_{InGaAlAs} and n_{InAlAs}. (b) Quantum efficiency with corresponding values of n_{InGaAlAs} and n_{InAlAs}.

Next we consider the effect of variation in thickness of DBM M_2. The calculated quantum efficiencies with $\pm 3\%$ deviation of InGaAlAs and InAlAs layer thicknesses are shown in Fig. 8. As the thickness of either the InGaAlAs or the InAlAs layer increases,

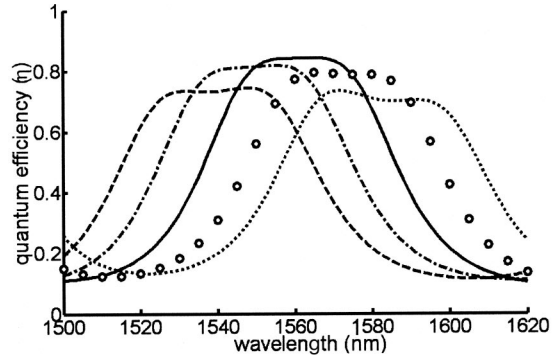

Fig. 8. Effect of variations in layer thickness of DBM M_2. Quantum efficiency with several thicknesses of InAlAs and InGaAlAs layers: 97% variation of the InAlAs layer and 100% of the InGaAlAs layer (dashed curve), 100% variation of the InAlAs layer and 100% of the InGaAlAs layer (solid curve), 103% variation of the InAlAs layer and 100% of the InGaAlAs layer (dotted curve), 100% variation of the InAlAs layer and 97% of the InGaAlAs layer (dashed–dotted curve), and 100% variation of the InAlAs layer and 103% of the InGaAlAs layer (circles).

Au	500 nm
Ti	5 nm
p+ InP	294.4 nm
i-InGaAs	467.6 nm
n+ InP	355.8 nm
InGaAlAs	139.4 nm
InAlAs x13	91.3 nm
InGaAlAs	249.0 nm
InAlAs	91.3 nm
InGaAlAs	139.4 nm
InAlAs x6	91.3 nm
InGaAlAs	69.7 nm
S.I. InP substrate	
SiN	134.7 nm
SiO_2	149.7 nm

(a)

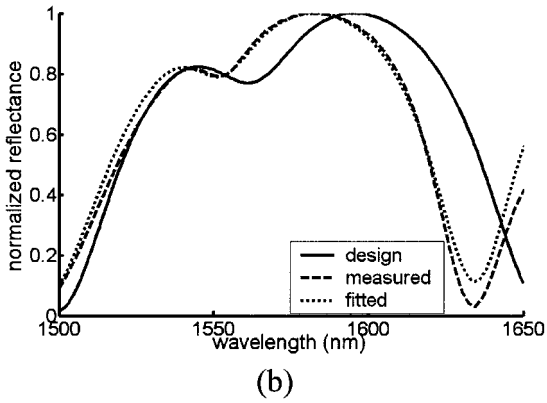

Fig. 9. (a) Schematic diagram of the layers of the fabricated device. (b) Normalized reflectance spectra of the design results, measured data, and optimization results of a fitted reflectance spectrum from 1500 to 1600 nm are shown; S.I., semi-insulating. We made the measurement and calculations by looking from the epitaxial side to the substrate without evaporation. The substrate side is unpolished.

the quantum efficiency shifts to a shorter wavelength because of a decrease of the total optical thickness of the device. In addition, the shape of the spectrum is distorted as the variation is extended, where the distortion is attributed to the mismatch of the first condition. We also observe that the distortion that results from variations in thicknesses of the InGaAlAs layers is worse than that of the InAlAs layers, as the deviation of total phase Φ caused by the variation of the InGaAlAs layers is larger than that of the InAlAs layers because $n_{\mathrm{InGaAlAs}} > n_{\mathrm{InAlAs}}$. In summary, we have found that, when our first optimization condition is not satisfied, distortion of the spectrum and smaller quantum efficiency result. In addition, this design is more sensitive to variations in the refractive index of M_2 than to variations in its thickness.

5. Fabrication and Characterization of the RCE PD

A RCE PD with the structure $H_2L(HL)^qH_1(LH)^pLS_2AS_1M_1$ with $p = 13$, $q = 7$, $H_1 = 249.0$ nm, $H_2 = 69.7$ nm, and $S_2 = 355.8$ nm was fabricated by metal-organic chemical-vapor deposition upon semi-insulating InP substrates. Because of backillumination, we added a two-layer antireflection coating, using SiO_2 ($n = 1.45$) and SiN ($n = 2.0$) with 149.7 and 134.7 nm at thicknesses of SiO_2 and SiN, respectively.[19] The growth multilayer structure is shown in Fig. 9(a).

Before the metallic layers are evaporated, the reflectance spectra of these epitaxial layers are characterized as shown in Fig. 9(b). We find that the measured spectrum shifts roughly 10 nm to a shorter wavelength than the designed calculation. In addition, the resonance dip at 1550 nm is slightly narrower than the designed dip. The fit is the simulation results including the dispersion of refractive indices for all the materials and with correcting factors of 1.017 for the InAlAs layer thickness, 0.984 for the InGaAlAs layer thickness, 0.998 for the n^+ and p^+ InP layers, and 1.019 for the i-InGaAs layer. The parameters are chosen to fit the measured spectrum from 1500 to 1600 nm.

Figures 10(a) and 10(b) show r_1, $r_2 \exp(-\alpha d)$, and Φ calculated by the design parameters and the optimized parameters fitted to the reflectance spectrum. As shown, we find that $r_2 \exp(-\alpha d)$ has a smaller value than expected and is not constant owing to the dispersion of the active layer. In addition, the spectrum of r_1 shifts to 1550 nm with a higher value than expected. Hence our second optimization condition is not perfectly satisfied. The spectrum of total phase Φ is similar to that of the design, except for its shift by 10 nm to a shorter wavelength. Therefore we expected that a smaller maximum and a rounder and narrower bandwidth would be obtained, similar to the performance described in the discussion above of the sensitivity that is due to variations in refractive index.

We measured the quantum efficiency of this device, utilizing a tungsten-halogen light source, spectrally resolved with a scanning monochrometer, with the signal detected by standard lock-in techniques. Figure 10(c) depicts the quantum-efficiency spectra of

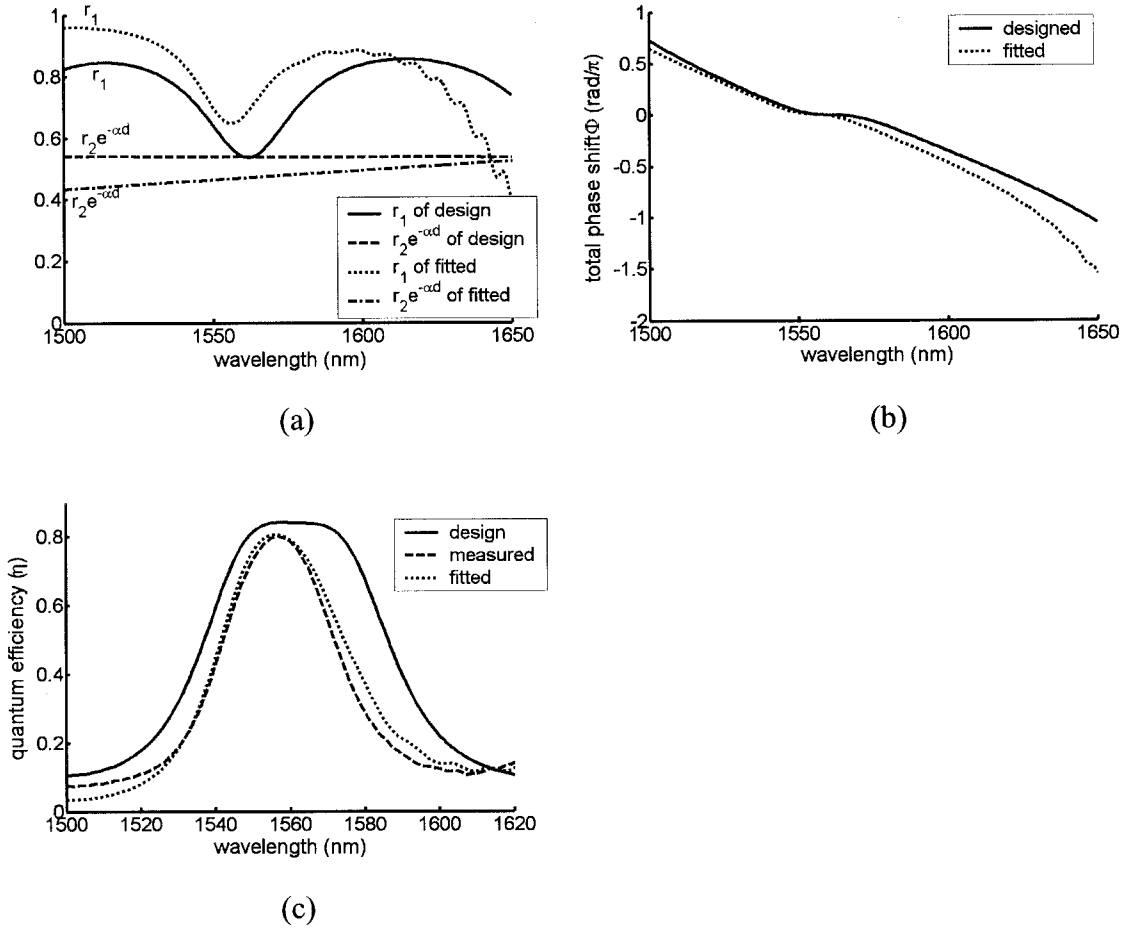

Fig. 10. (a) Relation of conditions (ii) (see text). The fitted curves were calculated by the optimized parameters obtained by fitting of the reflectance spectrum in Fig. 9(b). (b) Total phase Φ of the design and that calculated by the optimized parameters are shown. (c) Quantum efficiency of the design, measured and fitted by the optimized parameters.

the design calculated by Eq. (4), the measured data in the bias-free cases, and the simulation that uses parameters in the fitted case from Fig. 9(b) and calculated by Eq. (3). As shown in Fig. 10(c), the designed PD possesses high quantum efficiency at 1560 nm, with a value of 0.84. In addition, the FWHM of the quantum efficiency is ~54.74 nm, and a 0.02 dB drop (99.5%) in bandwidth is 13.27 nm. The measured data show a peak quantum efficiency at 1550 nm of 0.80 and a FWHM of 35.96 nm, and the width of the 0.02 dB drop is 3.42 nm, which are less than the designed results but are in relatively good agreement with results calculated with parameters fitted to the reflectance spectrum.

6. Conclusions

We have theoretically and experimentally demonstrated a RCE InGaAs p-i-n PD with broad and high quantum efficiency. By substituting an AD mirror for the standard Bragg mirror as the entrance mirror and controlling the slope of the round trip inside the active layer, we achieved both flattopped conditions and high quantum efficiency. By investigating a single-cavity AD mirror, we found that the spectral bandwidth of a RCE PD is determined by the width of the AD region of the mirror. In addition, not only the maximum of quantum efficiency but also the spectral bandwidth increases as the active layer's thickness increases. The spectral bandwidth can be engineered by introduction of a high-order spacer into the cavity of the AD mirror and by increasing the thickness of spacer S_2 to high order.

A design with a maximum quantum efficiency of 0.84 and a FWHM of 54.74 nm has been presented, fabricated, and characterized. Experimental results with a maximum quantum efficiency of 0.80 and a FWHM of 35.96 nm were obtained. The mismatch between the simulated design and the actual device is due to errors in fabrication of the layer thickness growth and to neglect of material dispersion in the design.

The authors acknowledge the support of the Defense Advanced Research Projects Agency, the National Science Foundation, the U.S. Air Force Office of Scientific Research, and the Photonics Technology Access Program. In addition, we thank Uriel Levy, Pang-Chen Sun, and Nelson Li for fruitful discussions.

References

1. K. Kishino, M. S. Unlu, J.-I. Chyi, J. Reed, L. Arsenault, and H. Morkoc, "Resonant cavity-enhanced (RCE) photodetectors," IEEE J. Quantum Electron. **27,** 2025–2034 (1991).
2. M. S. Unlu, K. Kishino, H. J. Liaw, and H. Morkoc, "A theoretical study of resonant cavity-enhanced photodetectors with Ge and Si active regions," J. Appl. Phys. **71,** 4049–4058 (1992).
3. M. S. Unlu and S. Strite, "Resonant cavity enhanced photonic devices," J. Appl. Phys. **78,** 607–39 (1995).
4. K. Liu, Y. Huang, and X. Ren, "Theory and experiments of a three-cavity wavelength-selective photodetector," Appl. Opt. **39,** 4263–4269 (2000).
5. H.-H. Tung and C.-P. Lee, "Design of a resonant-cavity-enhanced photodetector for high-speed applications," IEEE J. Quantum Electron. **33,** 753–60 (1997).
6. M. Gokkavas, G. Ulu, O. Dosunmu, R. P. Mirin, and M. S. Unlu, "Resonant cavity enhanced photodiodes with a broadened spectral peak," in *14th Annual Meeting of the IEEE Lasers and Electro-Optics Society* (Institute of Electrical and Electronics Engineers, 2001), Vol. 2, pp. 768–769.
7. S. Y. Hu, E. R. Hegblom, and L. A. Coldren, "Coupled-cavity resonant photodetectors for high-performance wavelength demultiplexing applications," Appl. Phys. Lett. **71,** 178–180 (1997).
8. Y. Zhong, Z. Pan, L. Li, Y. Huang, and X. Ren, "Proposition of a nearly rectangular response resonant cavity enhanced (RCE) photodetector," in *Semiconductor Optoelectronic Device Manufacturing and Applications*, D. Chen, ed., Proc. SPIE **4602,** 74–78 (2001).
9. F. Y. Huang, A. Salvador, X. Gui, N. Teraguchi, and H. Morkoc, "Resonant-cavity GaAs/InGaAs/AlAs photodiodes with a periodic absorber structure," Appl. Phys. Lett. **63,** 141–143 (1993).
10. A. Srinivasan, S. Murtaza, J. C. Campbell, and B. G. Streetman, "High quantum efficiency dual wavelength resonant-cavity photodetector," Appl. Phys. Lett. **66,** 535–537 (1995).
11. B. Temelkuran, E. Ozbay, J. P. Kavanaugh, G. Tuttle, and K. M. Ho, "Resonant cavity enhanced detectors embedded in photonic crystals," Appl. Phys. Lett. **72,** 2376–2378 (1998).
12. Y. H. Zhang, H. T. Luo, and W. Z. Shen, "Study on the quantum efficiency of resonant cavity enhanced GaAs far-infrared detectors," J. Appl. Phys. **91,** 5538–5544 (2002).
13. C. Li, Q. Yang, H. Wang, J. Yu, Q. Wang, Y. Li, J. Zhou, H. Huang, and X. Ren, "Back-incident SiGe–Si multiple quantum-well resonant-cavity-enhanced photodetectors for 1.3-μm operation," IEEE Photon. Technol. J. **12,** 1373–1375 (2000).
14. A. Thelen, *Design of Optical Interference Coatings* (McGraw-Hill, 1989), p. 20.
15. Y. V. Troitski, "Dispersion-free, multiple-beam interferometer," Appl. Opt. **34,** 4717–4722 (1995).
16. E. D. Palik, *Handbook of Optical Constants of Solids* (Academic, 1998), Vols. I and III.
17. W. Kowalsky and J. Mahnss, "Monolithically integrated InGaAlAs dielectric reflectors for vertical cavity optoelectronic devices," Appl. Phys. Lett. **59,** 1011–1012 (1991).
18. Y. Y. Troitski, "Dielectric mirrors with the anomalous dispersion of the reflection phase," Opt. Spectros. **77,** 503–506 (1994).
19. H. A. Macleod, *Thin-Film Optical Filters*, 3rd ed. (Institute of Physics, 2001).
20. M. J. Mondry, D. I. Babic, J. E. Bowers, and L. A. Coldren, "Refractive-indexes of (Al, Ga, In) As epilayers on InP for optoelectronic applications," IEEE Photon. Technol. Lett. **4,** 627–630 (1992).